This is a preprint, the final version is subject to change, of the American Mineralogist (MSA)
Cite as Authors (Year) Title. American Mineralogist, in press.
(DOI will not work until issue is live.) DOI: http://dx.doi.org/10.2138/am-2017-5704

Revision 1

Infrared Spectra of Carbonate Apatites:

Interpretation of Complex Asymmetric Stretch (ν_3) Region

Michael E. Fleet

Department of Earth Sciences, University of Western Ontario

London, Ontario N6A 5B7, Canada:

fax: 519-661-3198; e-mail: mfleet@uwo.ca

Running Title: Carbonate apatite

This is a preprint, the final version is subject to change, of the American Mineralogist (MSA)
Cite as Authors (Year) Title. American Mineralogist, in press.
(DOI will not work until issue is live.) DOI: http://dx.doi.org/10.2138/am-2017-5704

ABSTRACT

The complex asymmetric stretch (ν_3) region infrared (IR) spectrum of synthetic sodium- and carbonate-bearing hydroxylapatites (CHAP) has been interpreted using overlapped Gaussian distributions for individual carbonate ion species. There is now good agreement for the distribution of carbonate ions between phosphate (type B) and *c*-axis channel (type A) positions using three independent methods: X-ray structure site occupancies, out-of-plane bend (ν_2) band areas, and asymmetric stretch (ν_3) band areas; B/A ratios for a well-crystallized CHAP sample being 0.77, 0.78 and 0.75, respectively. The reported dominance of type B carbonate ions in bone mineral and dental enamel is attributed to the anomalous shift of type A band frequencies into the spectral region of type B, resulting from the substitution of Ca^{2+} by Na^{1+} in the nearest-neighbor cation shell of the channel carbonate ions. The infrared spectra show that the hydrogencarbonate (bicarbonate) ion in apatite crystals is a channel species, as are its room-temperature decomposition products, type A carbonate and labile (type L) carbonate. The research suggests that bone mineral crystals may actively communicate with body fluids through the apatite channel, pointing to a possible role for the apatite channel in mediating acid-base reactions in the body.

Key Words: apatite structure, carbonate ion, biomineralization, biological apatite, infrared spectra, CO_2 sequestration

This is a preprint, the final version is subject to change, of the American Mineralogist (MSA)
Cite as Authors (Year) Title. American Mineralogist, in press.
(DOI will not work until issue is live.) DOI: http://dx.doi.org/10.2138/am-2017-5704

INTRODUCTION

Carbonate-bearing hydroxylapatite is by far the most important biomineral, accounting for up to about 70 wt% of cortical bone and 97 wt% of dental enamel; typical carbonate contents for bone and enamel being 4.8 and 3.0 wt% CO_2, respectively (Elliott 2002). The carbonate content has a direct bearing on the growth and strength of bone (Liu et al. 2011), bone physiology, and development of bone prostheses, and it is the reservoir for controlling excess acidity and alkalinity in the human body (Bettice 1984; Green and Kleeman 1991; Rey et al. 2009). Fluoride-bearing hydroxylapatite is the important anticaries component of dental enamel (Brudevold et al. 1956), and carbonate-bearing fluorapatite and francolite are the dominant mineral varieties in phosphorites (McClellan and Lehr 1969).

In the present paper, the abbreviations HAP, FAP and CLAP refer to both ideal formulae and synthetic phases of hydroxylapatite, fluorapatite and chlorapatite compositions, respectively, and CHAP, CFAP and CCLAP are used similarly for the corresponding synthetic carbonate-bearing phases. The ideal formula of hydroxylapatite is $Ca_4Ca_6(PO_4)_6(OH)_2$, and the hexagonal structure can accommodate the carbonate ion in either the *c*-axis structural channel, where it substitutes for the hydroxyl ion (type A carbonate; A CHAP):

$$[^{A}CO_3 = 2(OH)] \quad (1)$$

or the apatite matrix, where it substitutes for the phosphate group (type B carbonate, B CHAP). This latter substitution requires charge balancing and may be complex; e.g.:

$$[Na + {}^{B}CO_3 = Ca + PO_4] \quad (2)$$

Both synthetic and natural carbonate apatites typically contain both type A and type B carbonate ions (AB CHAP).

Although the basic crystal structures of fluorapatite and hydroxylapatite have been

This is a preprint, the final version is subject to change, of the American Mineralogist (MSA)
Cite as Authors (Year) Title. American Mineralogist, in press.
(DOI will not work until issue is live.) DOI: http://dx.doi.org/10.2138/am-2017-5704

known since 1930 (Náray-Szabó 1930 and Mehmel 1930, respectively), the structural roles of the carbonate ion in biological apatite and francolite have remained elusive, due to the nanoscale crystal size, fragility and reactivity of nanocrystals extracted from bone tissue and phosphorites and their low degree of crystallinity. Progress made using analogue materials is reviewed in LeGeros (1991) and Elliott (1994, 2002), and an extended bibliography of more recent studies is given in Fleet et al. (2011). It was established in early studies (e.g., LeGeros et al. 1969) that the carbonate ion could be present both in the *c*-axis structural channel and as a substituent for the phosphate group, but more detailed structure analysis was limited again by nanoscale crystal size and low degree of crystallinity.

Recently, the accommodation of the carbonate ion in sodium-free CHAP (Fleet and Liu 2003, 2004, 2005; Fleet et al. 2004) and sodium-bearing CHAP, CCLAP and CFAP (Fleet and Liu 2007a, 2008a,b), has been investigated using the X-ray single-crystal structure method in conjunction with Fourier transform infrared spectroscopy (FTIR, IR) and single crystals grown from carbonate-rich melts at high *P*/*T*. CHAP compositions encompassed the composition fields of apatite in cortical bone and dental enamel (Elliott 2002; Fleet 2012). In an important application of the experimental results, the areas of out-of-plane bend (ν_2) IR bands were used to estimate the distribution of carbonate ions between the phosphate matrix and apatite structural channel (Fleet 2009; this is presently referred to as the IR(ν_2) method). In the present paper, the individual asymmetric stretch (ν_3) region bands are revealed for the first time using overlapped Gaussian distributions, giving carbonate ion proportions (B/A) consistent with the X-ray structure site occupancies and out-of-plane bend (ν_2) IR band areas, and providing an explanation for the troublesome discrepancy between the ν_2- and ν_3-region IR methods in bone and dental enamel research (e.g, Rey et al. 1989, 2009).

This is a preprint, the final version is subject to change, of the American Mineralogist (MSA)
Cite as Authors (Year) Title. American Mineralogist, in press.
(DOI will not work until issue is live.) DOI: http://dx.doi.org/10.2138/am-2017-5704

EXPERIMENTAL

Single crystals of sodium- and carbonate-substituted hydroxylapatite were synthesised at 0.5-1.0 GPa and 1200°C using a Depths of the Earth Company Quickpress piston-cylinder device and 3/4 inch assembly (Fleet and Liu 2007a). Starting compositions were prepared from analytical grade $CaHPO_4$, Na_2CO_3, $Ca(OH)_2$, and $CaCO_3$. These salts were mixed in stoichiometric proportions corresponding to an ideal carbonate apatite formula of $Ca_{10-y}Na_y[(PO_4)_{6-y}(CO_3)_y](OH)_2$ with $y = 2$ or 3 and excess fluid. The three apatite products investigated in this study were LM005 (with 8.2 wt% CO_2), LM006 (3.5 wt%) and LM002 (2.8 wt%): mineral formulae are based on electron microprobe analysis for major elements and X-ray structure site occupancies for CO_2 (Fleet and Liu 2007). Further details on crystal synthesis and characterization are given in Table 1. Carbonate ions were located, for LM005 and LM006, from difference electron density maps calculated after X-ray structure refinement of the basic apatite host structure and interpreted using model structures (Fleet et al. 2011).

Infrared spectra were collected with a Nicolet Nexus 670 FTIR spectrometer using KBr pellets, hand-separated crystals and unpolarized radiation. About 10 mg of apatite crystal product was first crushed and ground to a powder, then diluted in an agate mortar with 1 g of dry potassium bromide, and ground further under an IR heating lamp to a grain size less than 5 μm. Transparent discs were made under vacuum at a pressure of about 200 kg/cm^2. Important bands in the IR spectrum of apatite LM005 were identified from the peaks and shoulders in the envelope to the complex asymmetric stretch (ν_3) region and fitted to Gaussian profiles using a linear background over the limited spectral range investigated, and program BGAUSS (Tyliszcak 1992). The fitted spectrum of apatite LM005 was used as a template for the apatites with weaker spectral features, LM006 and LM002.

This is a preprint, the final version is subject to change, of the American Mineralogist (MSA)
Cite as Authors (Year) Title. American Mineralogist, in press.
(DOI will not work until issue is live.) DOI: http://dx.doi.org/10.2138/am-2017-5704

PREVIOUS RESEARCH

X-ray structures

The channel structure of sodium-bearing type AB CHAP LM005 (Fleet and Liu 2007a) is reproduced in Figure 1. The diffraction pattern of the type A CHAP from experiment PC71 (Table 1) is consistent with $P\bar{3}$ symmetry, a new space group for carbonate apatites (Fleet and Liu 2003), but the space group of all other carbonate apatites investigated is $P6_3/m$. The high apparent symmetry of carbonate apatite crystals is the result of disorder of the carbonate ion in the *c*-axis channel. There are six equivalent orientations for space group $P\bar{3}$ and twelve for $P6_3/m$: only one orientation is shown in Figure 1.

The carbonate ions are located in the *c*-axis channel by triclusters of Ca2 cations at unit-cell heights of $z \approx 1/4$ and $z \approx 3/4$. The X-ray structures show that the type A carbonate ion is oriented with two oxygen atoms close to the *c*-axis, and with the carbon atom and the third, off-axis, oxygen atom (O5) at a unit-cell height of $z \approx 0.5$. In type A CHAP, the plane of the carbonate ion is rotated about 14° counter clockwise from ideal orientation (Fleet et al. 2011), whereas in both sodium-free and sodium-bearing AB CHAP the rotation is clockwise, 7° for PC55 and 13° for LM005 (Fig. 1), moving the O5 oxygen atom closer to the channel wall.

The X-ray structure of apatite LM005 with $P6_3/m$ symmetry showed that the *c*-axis channel was fully occupied by carbonate ions, and only one carbonate ion orientation (that with two oxygen atoms close to the *c*-axis; Fig. 1) was recognized (Fleet and Liu 2007a). Small amounts of carbonate ions may have been present in other orientations in the apatite channel but not detected. Fleet and Liu (2005) concluded that the structural adjustments required to accommodate the bulky carbonate ion in the apatite channel of the $P\bar{3}$ structure of type A CHAP are complex, and include dilation of the channel at $z \approx 0.5$, constriction of the channel at $z \approx 0.0$,

contraction of the large cation polyhedron ($Ca1O_9$), and rotation of the PO_4 tetrahedron.

The type B carbonate ion remains poorly resolved in X-ray structures of carbonate apatites due to extensive overlap with oxygen atoms of the phosphate group. It was located close to a sloping face of the substituted phosphate tetrahedron, but tilted away from it in CCLAP and CHAP, with the tilt angle (ϕ) apparently increasing from -4(1)° in CFAP to +8(1)° in CCLAP and +18(2)° in CHAP (Fleet and Liu 2007a, 2008a,b), where detection limits are estimated and tilt angle is defined in more detail in Fig. 5.14 of Fleet (2014b). The result for CFAP is generally consistent with both polarized infrared measurements on francolite (~2°; Elliott 1964, 2002) and a neutron scattering study on sodium-bearing type B CHAP (~-5°; Wilson et al. 2004).

Fleet and Liu (2007a) reported that the substituents in synthetic type AB carbonate apatites and, possibly in all complex AB apatites as well, are present as a defect cluster. In the average structures of sodium-bearing AB carbonate apatites synthesized at high *P*/*T*, the off-axis oxygen atom O5 of a type A carbonate ion in the *c*-axis channel is prohibitively close at 1.1-1.2 Å to an O3 oxygen atom of a PO_4 phosphate group. This close O5-O3 interaction is eliminated in the local structure when the phosphate group is replaced by a type B carbonate ion (substitution 2) and the O3 oxygen atom in question is removed entirely from the structure, thus coupling one A and one B carbonate ion defect. This same distortion also results in an additional short Ca2-O interaction (indicated by the dashed line in Figure 1) but its contribution to the bonding sphere is uncertain.

Infrared spectroscopy

Reference carbonate band positions for carbonate apatites are given in Table 2, and selected spectra are reproduced in Figures 2 and 3. The carbonate component of the infrared spectrum of

a carbonate apatite with a single carbonate ion species generally consists of three bands; a strong symmetrical doublet band at 1600-1400 cm^{-1} for the asymmetric stretch (ν_3) mode and a weak singlet band at 880-870 cm^{-1} for the out-of-plane bend (ν_2) mode (Fig. 2). The symmetrical stretch (ν_1) mode is predicted but the band is buried in the strong phosphate stretch bands, and the band for the in-plane bend (ν_4) mode is characteristically not observed.

The asymmetric stretch (ν_3) mode is two-fold degenerate for the free carbonate ion, but this constraint is lifted for site symmetries lower than trigonal. In carbonate apatite spectra the site splitting results in two resolved bands, corresponding to a symmetric component (ν_{3a}) and an antisymmetric component (ν_{3b}; normal vibration modes of the free carbonate ion are illustrated in Madix et al. 1988). The latter vibration is stronger, theoretically (Nakamoto 1997), but this is not evident in the present IR spectra. The antisymmetric component is also generally the high-frequency vibration. Its location in IR spectra is quite variable, whereas the frequency of the symmetric component is fairly constant (i.e., within ±5 cm^{-1}) for channel carbonate ions across different carbonate apatites of the same or similar solid solution series (e.g., Elliott 1994; Suetsugu et al. 1998; Yi et al. 2014).

The asymmetric stretch (ν_3) mode appears as a single doublet for apatite with a single carbonate species (Table 2; Fig. 3c), but this spectral region is complex for most type AB carbonate apatites due mainly to overlap of the low-frequency limb of the type A doublet and the high-frequency limb of the type B doublet in the 1475-1445 cm^{-1} region. Moreover, bands for individual carbonate ion species are evident for sodium-free AB CHAP (Fig. 3a), but not for sodium-bearing AB carbonate apatites, including CHAP (Fig. 3b), CCLAP, CFAP, and all biological apatites. Figure 3 indicates that an anomalous feature in the IR spectra of these apatites, compared with sodium-free equivalents, is the shift of the band for the antisymmetric

This is a preprint, the final version is subject to change, of the American Mineralogist (MSA)
Cite as Authors (Year) Title. American Mineralogist, in press.
(DOI will not work until issue is live.) DOI: http://dx.doi.org/10.2138/am-2017-5704

component (ν_{3b}) of the channel carbonate ion to lower frequency. The resulting composite asymmetric stretch (ν_3) spectrum is dominated by two broad bands in the spectral region of the type B doublet, and results in a significant underestimation of the contribution of type A carbonate: e.g., type B carbonate is visually dominant in the spectrum of the sodium-bearing AB CHAP LM005 (Fig. 3b), but this apatite actually contains considerably more type A carbonate than type B (Table 1).

The singlet out-of-plane bend (ν_2) bands, on the other hand, are better resolved. They are located at characteristic positions (e.g., 880-878 cm^{-1} for type A carbonate ions, 873-871 cm^{-1} for type B, and 862-866 cm^{-1} for minor amounts of disordered labile (L) carbonate ions believed to be located in the apatite channel; Fleet 2009), and their band intensities are proportional to the amounts of A and B carbonate present. The proportionality of type A and type B carbonate was tested in Fleet (2009) by showing that the ratio B/A for IR band areas was in approximate one-to-one agreement with B/A calculated using the X-ray structure site occupancies (Table 1).

This is a preprint, the final version is subject to change, of the American Mineralogist (MSA)
Cite as Authors (Year) Title. American Mineralogist, in press.
(DOI will not work until issue is live.) DOI: http://dx.doi.org/10.2138/am-2017-5704

RESULTS AND DISCUSSION

Influence of alkali metals

The alkali metals are minor-trace components in compact bone and could be ignored in laboratory studies on the inorganic component of bone (known as bone mineral) were it not for the marked influence of sodium on the infrared spectra of carbonate apatites. The sodium cation enters the carbonate apatite structure to charge balance the substitution of phosphate by carbonate according to substitution reaction 2, modifying the local cation charge distribution in the *c*-axis channel and shifting the transition moment of the antisymmetric component (ν_{3b}) to lower frequency. This anomalous two-band asymmetric stretch spectrum is observed for all of the present synthetic sodium-bearing apatites (Fleet 2007a), as well as sodium-bearing AB CHAP synthesized at high temperature in other studies (Nelson and Featherstone 1982; Driessens et al. 1983), biological apatites, and synthetic potassium-bearing apatites (Verbeeck et al. 1995). The IR spectra for the potassium carbonate apatites and the present sodium analogue compounds are closely comparable (Fleet 2012, 2014a,b), showing that the principal factor shifting band positions is the local cation charge distribution in the *c*-axis channel, whereas cation size and other stereochemical details are relatively unimportant.

Verbeeck et al. (1995) investigated the development of type B carbonate in potassium AB CHAP through the exchange relationship:

$$[K + {}^{B}CO_3 = Ca + PO_4], \qquad (3)$$

with the channel carbonate sites remaining essentially fully occupied. Their IR spectra record diminution in the intensity of the high-frequency (ν_{3b}) component band for the type A doublet at ~1542 cm^{-1} and corresponding enhancement in intensity of the composite band at ~1475-1445 cm^{-1} with progressive increase in sodium and type B carbonate. This trend is interpreted to

This is a preprint, the final version is subject to change, of the American Mineralogist (MSA)
Cite as Authors (Year) Title. American Mineralogist, in press.
(DOI will not work until issue is live.) DOI: http://dx.doi.org/10.2138/am-2017-5704

represent the progressive substitution of divalent calcium in the nearest-neighbor Ca2 shell of the channel carbonate ions (Fig. 1). In other words, the band at ~1542 cm^{-1} represents the ν_{3b} mode for channel carbonate ions with the full complement of six nearest-neighbor calcium cations, and displacement of it to lower frequency represents channel carbonate ions with fewer than six nearest-neighbor calcium cations and Ca2 sites occupied by a sodium cation or cation vacancy.

Mobility in apatite channel

Information relevant to the reactivity of biological apatite in living systems has been provided by several room-pressure experiments on CHAP crystals that resulted in profound compositional changes within the apatite channel, leaving the type B component in the calcium carbonate-phosphate matrix essentially unchanged (Fleet 2012, 2014b). The most interesting of these followed the aging of high *P*/*T* hydrogencarbonate (bicarbonate)-bearing type AB CHAP crystals at room temperature and 110°C, from progressive change in their IR spectra (Fleet 2012; Fleet and Liu 2007b). The out-of-plane bend (ν_2) region of the infrared spectrum of hydrogencarbonate-bearing CHAP has four resolved bands, three for carbonate ions (A, B and labile, L) and a new band at 837 cm^{-1} representing vibration of the CO_3 cluster in the hydrogencarbonate (bicarbonate) ion (HCO_3^{1-}). Significantly, the 837 cm^{-1} band disappeared completely on aging quenched products for up to 283 days at room-temperature and 55 days at 110°C. Using change in IR(ν_2) band areas, the loss of hydrogencarbonate was marked by concomitant increase in the proportion of type A and type L carbonate, with the proportion of type B carbonate and total carbonate remaining essentially unchanged (Table 3). Type L carbonate is present in minor amounts and is represented in IR spectra as a low frequency shoulder to the dominant type B band, at 864-866 cm^{-1} (Fleet 2014b). A labile carbonate ion

This is a preprint, the final version is subject to change, of the American Mineralogist (MSA)
Cite as Authors (Year) Title. American Mineralogist, in press.
(DOI will not work until issue is live.) DOI: http://dx.doi.org/10.2138/am-2017-5704

component in CHAP and biological apatites is well established in the literature (Rey et al. 1989, 1991, 2009) and widely believed to represent a surface or disrupted carbonate ion species. In the present study, the labile (L) component is thought to be largely a reactive channel species due to the quantitative change in proportion of carbonate species on aging quenched high *P*/*T* CHAP. The change in proportions on aging reported in Table 3 suggest that: (1) The type B carbonate is bound firmly in the calcium carbonate-phosphate matrix; (2) The hydrogencarbonate and labile carbonate components are channel species; and (3) The decomposition of the hydrogencarbonate ion takes place exclusively in the apatite channel.

The change in proportions of the carbonate species also suggest that the carbonate ions formed on aging do not appear to be mobile in the apatite channel at room temperature; i.e., they do not leave the crystal system. Instead, the crystals progressively dehydrate through reactions simplified as:

$$[HCO_3^-] + [OH^-] \rightarrow H_2O + [CO_3^{2-}], \qquad (4)$$

where HCO_3^-, OH^- and CO_3^{2-} are bound species. Drying times for nanocrystals are estimated to be within order-of-magnitude agreement with the 2 to 24 hours estimated for the interactions between extracellular and skeletal carbon dioxide in the maintenance of acid-base homeostasis and mediation of metabolic acidosis (Neuman et al. 1968; Poyart et al. 1975a,b; Bettice 1984).

Interpretation of ν_3-region spectra

The complex asymmetric stretch (ν_3) region of the IR spectrum of sodium-bearing and biological carbonate apatites is usually interpreted to indicate the dominant presence of type B (matrix) carbonate (e.g., Rey et al. 2009; Elliott 1994). Prior to the present study, no explanation has been offered for the weak carbonate absorption beyond 1500 cm^{-1} that characterizes this spectrum (cf.,

Fig. 3b), other than a low content of type A (channel) carbonate.

The present interpretation of the complex ν_3 region of sodium-bearing carbonate apatite recognizes the near constancy of the frequency of the symmetric vibration component (ν_{3a}) for type A (channel) carbonate in given apatite composition series, and the potential for wide variation in the frequency of corresponding antisymmetric components (Elliott 1994). Elliott commented that the "… variability of ν_{3b} and near constancy of ν_{3a} have been linked to the fact that their transition moments are parallel and perpendicular respectively to the direction of greatest dimensional change, which is perpendicular to the *c*-axis…".

Six IR absorption bands were identified for each of the three CHAP samples investigated (Fig. 4). The resulting band frequencies, widths and areas are summarized in Table 4. Note that resolution of the X-ray structures and quality of the IR spectra diminish rapidly with decreasing carbonate content in the sequence LM005 > LM006 > LM002, to the extent that apatite LM002 did not yield useful X-ray structure data and its composite asymmetric stretch (ν_3) profile was ragged. The refined parameters for the six bands in Table 4 accounted for greater than 99.5% of the area of the complex asymmetric stretch (ν_3) region of apatite LM005. Because the fitting procedure was underdetermined, band widths were set by iteration allowing band frequencies and half widths (FWHH) to be calculated by open least-squares refinement. The convergence of the refinements was tested by recovering the fit for LM005 after randomly off-setting all band frequencies by up to ±20 cm^{-1}.

Bands 3 and 5 in the fitted spectrum for apatite LM005 (Table 4; Fig. 4) appear to correspond, respectively, to the symmetric (ν_{3a}) and antisymmetric (ν_{3b}) components of the type B carbonate ion doublet, because this assignment has numerous counterparts in the literature (Table 2): note that the areas (absorption intensities) of these two bands are more or less equal as

291 required by theory. The type B carbonate ion environment is formed by the removal of one
292 oxygen atom from a phosphate tetrahedron and subsequent collapse of the surrounding structure
293 (Fleet and Liu 2007a). Although the structural details have not been determined for apatite
294 LM005, one can assume, from the similar IR parameters for all three sodium-bearing apatites
295 investigated (Table 4) and its lack of participation in channel reactions (Table 3), that the type B
296 carbonate ion represents a stable configuration; i.e., the type B carbonate ion is firmly bound in
297 the apatite matrix, in a reproducible manner.

298 Some caution is introduced here because multiple type B environments have been
299 reported in asymmetric stretch (ν_3) spectra of other carbonate-bearing apatites: e.g., the spectrum
300 of a fluorapatite of metamorphic origin from Wilberforce, Ontario, has bands at 1406, 1427,
301 1449, and 1458 cm^{-1}, consistent with the presence of at least two different stereochemical
302 environments for type B carbonate (Tacker 2008). It is noted also that the formula amount of
303 sodium in apatite LM005 does exceed that of type B carbonate (Table 1) in apparent
304 disagreement with substitution reaction 2, but this discrepancy may not be too significant in light
305 of experimental errors, crystal imperfections and expected partitioning of a portion of the sodium
306 content into the large cation site (Ca1) of the apatite structure.

307 The band assignments for type A (channel) carbonate species in apatite LM005 have
308 been made using the reference band positions in Table 2 and, following Elliott (1994), the
309 assumption that band 4 (Table 4; Fig. 4) is common to most or all of the channel carbonate ion
310 species and represents the total absorption from the symmetric vibration components (ν_{3a}). It is
311 further assumed that bands 2 and 6 are the antisymmetric components (ν_{3b}) for two separate type
312 A (channel) species; i.e., for two distinct carbonate ion environments in the apatite channel,
313 which are presently labelled type Ab for bands 2 and 4 at 1501 and 1449 cm^{-1} and type Ac for

bands 6 and 4 at 1389 and 1449 cm^{-1}, respectively.

The X-ray diffraction study of apatite LM005 did not reveal evidence for more than one stereochemical environment of the type A (channel) carbonate ion. This observation suggests that if several type A carbonate ion sites are present they must have similar coordination geometries but different nearest-neighbor Ca2 cation site populations; i.e., (6Ca), (5Ca1Na), (5Ca1□), etc., representing progressive reduction of the Ca2 cation charge binding the carbonate ion in the apatite channel (cf., Fig. 1). This situation is facilitated by the similar ionic radii of Ca^{2+} and Na^{1+} cations in given coordinations. Stepwise reduction in the nearest-neighbor Ca2 cation charge would seem to account qualitatively for the progressive downward shift in frequency of the antisymmetric components (ν_{3b}) of the carbonate species in the apatite channel. Of course, a quantitative analysis would have to take into account all contributions to Ca2-O bond strengths as well as change in the reduced mass of the vibration system.

Thus, one can make a reasonable guess at the local stereochemical environments of these channel carbonate species. Bands 2 and 4 at 1501 and 1449 cm^{-1}, respectively, have counterparts in the sodium-bearing AB CHAP studied by Nelson and Featherstone (1982; present Table 2) and, more generally, must characterize type Ab carbonate ions in sodium-bearing AB CHAP. These two bands most likely represent the fingerprint for the channel carbonate ion species with a nearest-neighbor cation configuration on Ca2 sites of five calcium and one sodium cations; i.e., (5Ca1Na), with three cations at $z \approx 1/4$ and three at $z \approx 3/4$ in the configuration of a trigonal antiprism (Fig. 1). Indeed, type Ab was expected to be the dominant carbonate ion species in the apatite channel, and its relatively low proportion in apatite LM005 is somewhat surprising.

Reconstruction of the local environment of the carbonate species Ac (bands 6 at 1389 cm^{-1} and 4 at 1449 cm^{-1}) is somewhat problematical on account of the large downward shift in

337 frequency of the antisymmetric component, from 1501 cm^{-1} for Ab carbonate species to 1389
338 cm^{-1} for Ac. Thus, absorption band 6 is assigned tentatively to the antisymmetric component
339 (ν_{3b}) of a new channel species with doublet bands at 1389 and 1449 cm^{-1}, but must correspond to
340 a significant reduction in charge on the nearest-neighbor Ca2 cation site. The assignment of the
341 corresponding symmetric limb (ν_{3a}) to band 4, however, is made with some confidence even
342 though it is overlapped by type Ab absorption, because the type Ac doublet makes a major
343 contribution to the spectrum of apatite LM005 (Table 4). Almost 50% of the intensity of band 4
344 would be unaccounted for in the absence of the contribution from the Ac doublet. A complete
345 understanding of the large frequency shift for the antisymmetric component (ν_{3b}) from type Ab
346 carbonate to type Ac must await theoretical calculation on the effects of substitution of calcium
347 cations by sodium or vacancies. However, this downward shift would seem to be consistent with
348 a Ca2 population of either (5Ca1□) or (4Ca2Na) and, perhaps, a high P/T synthesis as well. Note
349 that the proportion of type Ac carbonate ions decreases markedly with decrease in total carbonate
350 content, down to a background amount in apatite LM002 (Table 4). Also, band 6 which
351 characterizes type Ac carbonate is not present in IR spectra of sodium-free CHAP (Fleet et al.
352 2004) and only weakly present in biological apatites.
353 Following the trend in frequency shift for bands 2 and 6 (at 1501 and 1389 cm^{-1},
354 respectively), band 1 at 1536 cm^{-1} could be interpreted as the antisymmetric component (ν_{3b}) of a
355 third channel species, labelled type Aa with components at 1536 and 1449 cm^{-1} for bands 1 and
356 4, respectively, corresponding to a minor residual amount of channel carbonate ions in a cage of
357 six nearest-neighbor calcium cations on Ca2 sites; i.e., (6Ca). This is the local environment of
358 the type A carbonate ion in sodium-free A CHAP, and its IR spectrum (Fig. 3) is again consistent
359 with CHAP examples in Table 2. This Aa assignment is supported by the broadscan spectrum of

This is a preprint, the final version is subject to change, of the American Mineralogist (MSA)
Cite as Authors (Year) Title. American Mineralogist, in press.
(DOI will not work until issue is live.) DOI: http://dx.doi.org/10.2138/am-2017-5704

annealed carious enamel in Arends and Davidson (1975; present Fig. 2), which has a prominent absorption peak at 1545 cm^{-1}.

In summary, the fitted IR spectrum of the sodium-bearing CHAP LM005 reveals evidence of at least three channel carbonate ion species, which are presently labelled type Aa, type Ab and type Ac. These have the same, or similar, atomic configuration in the channel and are distinguished by a progressive shift in the position of the IR band for the antisymmetric component (ν_{3b}), from 1536 cm^{-1} for type Aa, to 1501 cm^{-1} for type Bb, and 1389 cm^{-1} for type Ac.

The labels used for channel carbonate ion species in this paper on sodium-bearing CHAP should not to be confused with labels used in earlier studies on sodium-free CHAP (e.g., Fleet et al. 2011), where two separate orientations of the channel carbonate ion were recognized , and labelled type A (occasionally type A1) and type A2. Type A carbonate in sodium-free CHAP is oriented with two oxygen atoms close to the *c*-axis as in type Aa, type Ab, and type Ac of this study (Fig. 1), whereas type A2 has only one oxygen atom close to the *c*-axis. IR spectra showing characteristic bands for A and A2 carbonate in sodium-free CHAP are reproduced in Fig. 3.

A complication here in using band areas to quantify the proportion of channel carbonate is that the sum of the areas of the three proposed type A antisymmetric components (i.e., bands 1, 2 and 6) exceeds the area of the symmetric components of band 4, by 10.2 to 8.4 arbitrary units for apatite LM005 (Table 4); this discrepancy being significantly larger than the expected experimental errors. Alternatively, when the summation includes only bands 2 and 6 (type Ab and type Ac species), the agreement between the sums of the symmetric (ν_{3a}) and antisymmetric (ν_{3b}) components improves to good; i.e., 8.6 to 8.4. This latter interpretation suggests that most

383 of the absorption assigned to the type Aa carbonate species in the LM005 spectrum (Table 4) is
384 spurious and not associated with the apatite lattice. The intensity of band 1 is undoubtedly
385 enhanced by background contributions from nearby H_2O bend vibrations and phosphate stretch
386 vibrations that dominate all calcium phosphate apatite IR spectra (e.g., Fig. 2). Correction has
387 not been attempted for these interferences, which would make a considerable contribution to the
388 intensity of weak bands in the complex asymmetric stretch (ν_3) region.

389 The present interpretation of the asymmetric stretch (ν_3) spectrum of the quenched high
390 *P*/*T* CHAP LM005 provides an adequate explanation for the anomalous region at 1475-1445 cm^{-1}
391 in the IR spectrum of alkali-bearing carbonate hydroxylapatites. Basically, it is predicted that
392 the substitution of calcium by sodium reduces the total positive charge on the nearest-neighbor
393 Ca2 cation cage, shifting the antisymmetric limb (ν_{3b}) of the asymmetric stretch vibration (ν_3) to
394 lower frequency, and leaving the frequency of the symmetric component (ν_{3a}) essentially
395 unchanged.

396 Deconvolution of the asymmetric stretch (ν_3) spectrum using overlapped Gaussian
397 distributions (Fig. 4; Table 4; presently referred to as the IR(ν_3) method) shows that type A
398 carbonate exceeds type B by about 25% in apatite LM005. This result is in agreement with
399 previous estimates for the proportion of these two carbonate species from the X-ray structure site
400 occupancies (Fleet and Liu 2007a) and out-of-plane bend (ν_2) band areas (Fleet 2009).
401 Comparison figures for the ratio of type B to type A carbonate (B/A) are 0.78, 0.75 and 0.77, for
402 IR(ν_2), IR(ν_3) and XRD methods, respectively (Tables 1 and 4), where B is total carbonate
403 substituting for phosphate and A is total carbonate in the apatite channel. The results for apatite
404 LM006 are more divergent, but still yield agreement within the uncertainties of the experimental
405 data and IR(ν_3) method.

This is a preprint, the final version is subject to change, of the American Mineralogist (MSA)
Cite as Authors (Year) Title. American Mineralogist, in press.
(DOI will not work until issue is live.) DOI: http://dx.doi.org/10.2138/am-2017-5704

Several different calculation schemes for the ratio B/A are presented in Table 4. The preferred calculation excludes a channel contribution from band 1, and a third procedure using only the information for bands 3, 4 and 5 is recommended where IR data are limited. In this study experimental errors increase markedly with decrease in total carbonate content and quality of IR spectra. Reproducibility is estimated in the most favorable cases as ±3% of the ratio B/A for LM005 and ±4% for LM006, increasing to beyond ±10% for LM002. Note that absolute amounts of carbonate in specific structural sites of apatite are obtained only by X-ray structure analysis, and the quality of these data depends one-to-one on the quality of the single crystal products used. In their classic study, Libowitzky and Rossman (1996) concluded that in most circumstances accurate determination of absorbance and/or concentration in anisotropic material cannot be performed by measurement with unpolarized radiation, unoriented samples and the KBr powder pellet technique, and was not attempted in this study. Instead, relative carbonate contents were obtained by measuring band areas over a limited spectral interval, and comparing the ratio B/A with absolute amounts of carbonate from single-crystal X-ray structure site occupancies. Finally, the good agreement between the two IR methods and XRD site occupancies is confirmation that differences in molar absorption coefficient for matrix (B) and channel (A) carbonate ions did not introduce significant error to the present estimation of B/A ratio.

Biological apatite

Nanoscale crystals of bone mineral are platy on (100) and tend to be oriented with the *c*-axis parallel or sub-parallel to the long axis of bones (Palmer et al. 2008), but otherwise are similar in chemical composition and structure to the sodium-bearing CHAP samples LM006 and LM005

(Fleet and Liu 2007a; Fleet 2014b). The nanoscale mineral crystals are too small and lack sufficient crystal quality to yield meaningful structural information using diffraction methods. Given these limitations, synthetic CHAP preparations have proven to be indispensable analogue materials for bone mineral and other biological apatites, especially for interpreting the results of chemical spectroscopy and in vitro experimentation. The most relevant products of the present extensive project on the crystal chemistry of bone mineral are apatites LM006 and LM005. Crystals of apatite LM006 have similar carbonate and sodium contents to bone mineral (cortical bone) and dental enamel, and LM005 crystals have the highest carbonate content and yielded the most detailed structure analysis. The presently proposed structure of bone mineral and dental enamel is supported by similarities with sodium-bearing AB CHAP in chemical composition (Fleet 2012), X-ray powder diffraction patterns, and IR spectra, taking into account that the IR spectra and powder patterns for the biological materials are degraded by low degree of crystallinity and nanocrystalline grain size (LeGeros 1991), and their asymmetric stretch (ν_3) IR spectra are partly obscured by amide bands from soft tissue contamination (e.g., Verdelis et al. 2007; Farlay et al. 2010). In more detail, the biominerals are expected to have a higher content of water, hydroxyl and type Aa carbonate ions and, perhaps a minimal content of type Ac carbonate ions compared with their synthetic equivalents (cf., Fig. 2), with type Ab carbonate ions dominant.

The overall similarity of the infrared spectra for biological apatite and sodium-bearing AB CHAP is especially reassuring, given that carbonate IR spectra are sensitive to slight change in the nearest-neighbor cation charge field and the extreme thinness reported for bone mineral crystals might be expected to signal a major role for the crystal surface in the chemistry of this apatite. The good agreement between the asymmetric stretch (ν_3) spectra for human enamel and

apatite LM005 (Elliott 1994; Arends and Davidson 1975; present Fig. 2) is confirmation that the stereochemical environments of the A and B carbonate ions are similar, respectively, in biological and synthetic carbonate apatites. Other literature examples (e.g., Farlay et al. 2010) support the suggestion that the shift to lower frequency of the antisymmetric component(s) (ν_{3b}) for type A carbonate is a characteristic feature of biological apatites, and the resulting overlap with type B bands has led to misleadingly low estimates for the type A carbonate content in early studies on bone mineral and dental enamel. Fitted out-of-plane bend (ν_2) and asymmetric stretch (ν_3) spectra show that type A carbonate is invariably present in significant amounts in biological apatites (Paschalis et al. 1996; Verdelis et al. 2007), as it is in sodium-bearing AB CHAP.

Quantification of the proportion of matrix (type B) and channel (type A) carbonate ions (B/A) in apatites is obtained most readily from the fitted band areas of out-of-plane bend (ν_2) spectra. This method was calibrated independently by the X-ray structures for synthetic carbonate apatites (Fleet 2009). The present study shows that quantitative information on the distribution of carbonate species between type B and type A structural sites (B/A) can be obtained also by deconvoluting the complex asymmetric stretch (ν_3) IR spectra using overlapped Gaussian distributions. There is now good agreement between three independent methods (out-of-plane bend (ν_2), asymmetric stretch (ν_3) and X-ray structure) for determination of the proportions of carbonate species in CHAP (Fleet 2009; Table 4).

It has been known for some time that the carbonate content of bone is the reservoir for controlling excess acidity in the body (Bettice 1984; Green and Kleeman 1991; Rey et al. 2009). In particular, in vivo experiments have shown that a considerable fraction of the carbonate associated with bone (about 30-40 %; Neuman and Mulryan 1967; Poyart et al. 1975a,b) is exchangeable with carbon species in body fluids. This exchangeable fraction is believed to be

This is a preprint, the final version is subject to change, of the American Mineralogist (MSA)
Cite as Authors (Year) Title. American Mineralogist, in press.
(DOI will not work until issue is live.) DOI: http://dx.doi.org/10.2138/am-2017-5704

hydrogencarbonate (bicarbonate) located either in the hydration shell or surface layer of the carbonate hydroxylapatite nanocrystals, although these suggestions have not been confirmed by subsequent study.

The synthetic hydrogencarbonate- and sodium-bearing AB CHAP crystals (Fleet and Liu 2007b) show that the apatite channel is a second, and possibly alternative, location for hydrogencarbonate ions associated with bone mineral nanocrystals. The limited literature studies in the infrared out-of-plane bend (ν_2) region reveal appreciable amounts of type A and disordered labile carbonate ions in apatite extracted from bone and dental enamel (Rey et al. 1989, 1991; Elliott 2002). There are sufficient channel carbonate ions in biological apatite crystals to account for the fraction of exchangeable CO_2 reported by Neuman and Mulryan (1967) and Poyart et al. (1975a,b), especially if the labile carbonate ions are assumed to be channel species. The observations on change in the proportion of carbonate and hydrogencarbonate (bicarbonate) species on aging (Fleet 2012; present Table 3) point to a possible role for the apatite channel in mediating acid-base reactions in the body (Bushinsky et al. 2002). It is suggested in this paper that channel constituents may account for a considerable proportion of the carbonate ions required for acid-base homeostasis and mediation of mild acidosis, possibly by consuming and releasing protons through the simplified solid-state reaction:

$$H^+_{aq} + [CO_3^{2-}] \leftrightarrow [HCO_3^-], \qquad (5)$$

where carbonate and hydrogencarbonate ions are species bound in the apatite channel and the proton migrates in the channel from or to the extracellular fluid. For the forward reaction, the excess positive charge in the channel wall is dissipated in the surrounding structure and eventually neutralized by the release of a Na^+ counter ion into the extracellular fluid or hydration shell.

This is a preprint, the final version is subject to change, of the American Mineralogist (MSA)
Cite as Authors (Year) Title. American Mineralogist, in press.
(DOI will not work until issue is live.) DOI: http://dx.doi.org/10.2138/am-2017-5704

IMPLICATIONS

Hydroxylapatite is the most important biomineral and is actively studied in biomaterials research: this mineral is a true bridge between earth material science and the medical sciences. But progress in understanding the crystal chemistry of apatite biomaterials, and their participation in physiological processes, has been limited by their nanoscale crystal size and poor crystal quality. A major problem has been disagreement on the relative proportions of channel (type A) and phosphate (type B) carbonate present, with the latter generally favoured as the reactive species. This paper deconvolutes the complex asymmetric stretch (ν_3) region of the infrared spectra of synthetic sodium-bearing carbonate apatite crystals, revising previous procedures that over-estimated the contribution of type B carbonate. The research suggests that bone mineral nanocrystals may actively communicate with body fluids through the apatite channel, pointing to a possible role for the apatite channel in mediating acid-base reactions in the body. This research should provide a platform for future geochemical and physiological experiments on carbonate apatites.

ACKNOWLEDGEMENTS

I thank Xi Liu for crystal synthesis and FTIR measurements, Chris Tacker and a second unnamed reviewer for helpful comments, and the Natural Sciences and Engineering Research Council of Canada for financial support.

519 **REFERENCES CITED**

520 Arends, J., and Davidson, C.L. (1975) HPO_4^{2-} content in enamel and artificial carious lesions.
521 Calcified Tissue Research, 18, 65-79.
522 Baxter, J.D., Biltz, R.M., and Pellegrino, E.D. (1966) The physical state of bone carbonate: A
523 comparative infra-red study in several mineralized tissues. The Yale Journal of Biology and
524 Medicine, 38, 456-470.
525 Bettice, J.A. (1984) Skeletal carbon dioxide stores during metabolic acidosis. American Journal
526 of Physiology, 247, F326-F330.
527 Bonel, G. (1972) Contribution à l'étude de la carbonatation des apatites. I. - Synthèse et étude
528 des propriétés physico-chimiques des apatites carbonatées du type A. Annales de Chimie,
529 (Paris, France), 7, 65-88.
530 Brudevold, F., Gardner, D.E., and Smith, F.A. (1956) Distribution of fluorine in human enamel.
531 Journal of Dental Research, 35, 420-429.
532 Bushinsky, D.A., Smith, S.B., Gavrilov, K.L., Gavrilov, L.F., Li, J., and Levi-Setti, R. (2002)
533 Acute acidosis-induced alteration in bone bicarbonate and phosphate. American Journal of
534 Physiology- Renal Physiology, 283, F1091-F1097.
535 Carlström, D. (1968) Mineralogical carbonate-containing apatites. In W.E. Brown, and R.A.
536 Young, Eds., Proceedings of International Symposium on Structural Properties of
537 Hydroxyapatite and Related Compounds, Gaithersburg, Maryland, Chap. 10.
538 Driessens, F.C.M., Verbeeck, R.M.H., and Heijligers, H.J.M. (1983) Some physical properties of
539 Na- and CO_3-containing apatites synthesized at high temperatures. Inorganica Chimica
540 Acta, 80, 19-23.
541 Elliott, J.C. (1964) The interpretation of the infra-red absorption spectra of some carbonate-

containing apatites. In R.W. Fearnhead and M.V. Stack, Eds., Tooth Enamel: Its Composition, Properties, and Fundamental Structure, pp. 20-22. John Wright & Sons Bristol, UK.

Elliott, J.C. (1994) Structure and Chemistry of the Apatites and Other Calcium Orthophosphates, 389 p. Elsevier, Amsterdam.

Elliott, J.C. (2002) Calcium phosphate biominerals. In M.J. Kohn, J. Rakovan, and J.M. Hughes, Eds., Phosphates, pp. 427-453. Reviews in Mineralogy and Geochemistry, 48, Mineralogical Society of America, Washington, D.C.

Farlay, D., Panzcer, G., Rey, C., Delmas, P.D., and Boivin, G. (2010) Mineral maturity and crystallinity index are distinct characteristics of bone mineral. Journal of Bone and Mineral Metabolism, 28, 433-445.

Fleet, M.E. (2009) Infrared spectra of carbonate apatites: ν_2-region bands. Biomaterials, 30, 1473-1481.

Fleet, M.E. (2012) The carbonate ion in hydroxyapatite and biological apatite. In Heimann, R.B., Ed., Calcium Phosphate: Structure, Synthesis, Properties, and Applications, pp. 41-61, Nova Science Publishers, New York.

Fleet, M.E. (2014a) Distribution of carbonate ions in biological apatite and excess fluorine in francolite. In Iafisco, M., Delgado-López, J.M., Eds., Apatite: Synthesis, Structural Characterization and Biomedical Applications, pp. 103-122, Nova Science Publishers, New York.

Fleet, M.E. (2014b) Carbonated Hydroxyapatite: Materials, Synthesis, and Applications, 268 p, Pan Stanford Publishing, Singapore .

Fleet, M.E., and Liu, X. (2003) Carbonate apatite type A synthesized at high pressure: new space

group ($P\bar{3}$) and orientation of channel carbonate ion. Journal of Solid State Chemistry, 174, 412-417.

Fleet, M.E., and Liu, X. (2004) Location of type B carbonate ion in type A-B carbonate apatite synthesized at high pressure. Journal of Solid State Chemistry, 177, 3174-3182.

Fleet, M.E., and Liu, X. (2005) Local structure of channel ions in carbonate apatite. Biomaterials, 26, 7548-7554.

Fleet, M.E., and Liu, Xi (2007a) Coupled substitution of type A and B carbonate in sodium-bearing apatite. Biomaterials, 28, 916-926.

Fleet, M.E., and Liu, Xi (2007b) Hydrogen-carbonate ion in synthetic high-pressure apatite. American Mineralogist, 92, 1764-1767.

Fleet, M.E., and Liu, Xi (2008a) Accommodation of the carbonate ion in fluorapatite synthesized at high pressure. American Mineralogist, 93, 1460-1469.

Fleet, M.E., and Liu, Xi (2008b) Type A-B carbonate chlorapatite synthesized at high pressure. Journal of Solid State Chemistry, 181, 2494-2500.

Fleet, M.E, Liu, X., and King, P.L. (2004) Accommodation of the carbonate ion in apatite: An FTIR and X-ray structure study of crystals synthesized at 2-4 GPa. American Mineralogist, 89, 1422-1432.

Fleet, M.E., Liu, X., and Liu, Xi (2011) Orientation of channel carbonate ions in apatite: Effect of pressure and composition. American Mineralogist, 96, 1148-1157.

Green, J., and Kleeman, C.R. (1991) Role of bone in regulation of systemic acid-base balance. Kidney International, 39, 9-26.

LeGeros, R.Z. (1991) Calcium Phosphates in Oral Biology and Medicine, 201 p., Karger, Basel.

LeGeros, R.Z., Trautz, O.R., Klein, E., and LeGeros, J.P. (1969) Two types of carbonate substitution in the apatite structure. Experimentia, 25, 5-7.

Libowitzky, E., and Rossman, G.R. (1996) Principles of quantitative absorbance measurements in anisotropic cystals. Physics and Chemistry of Minerals, 23, 319-327.

Liu, Xi, Shieh, S.R., Fleet, M.E., Zhang, L., and He, Q. (2011) Equation of state of carbonated hydroxylapatite at ambient temperature up to 10 GPa: Significance of carbonate. American Mineralogist, 96, 74-80.

Madix, R.J., Solomon, J.L., and Stöhr, J. (1988) The orientation of the carbonate anion on Ag(110). Surface Science, 197, L253-L259.

McClellan, G.H., and Lehr, J.R. (1969) Crystal chemical investigation of natural apatites. American Mineralogist, 54, 1374-1391.

Mehmel, M. (1930) Über die Struktur des Apatits. Zietschrift fur Kristallographie, 75, 323-331.

Nakamoto, K. (1997) Infrared and Raman Spectra of Inorganic and Coordination compounds. Part A: Theory and Applications in Inorganic Chemistry, 387 p., 5th edit. (John Wiley, New York).

Náray-Szabó, S. (1930) The structure of apatite $(CaF)Ca_4(PO_4)_3$. Zietschrift fur Kristallographie, 75, 387-398.

Nelson, D.G.A., and Featherstone, J.D.B. (1982) Preparation, analysis, and characterization of carbonated apatites. Calcified Tissue International, 34, S69-S81.

Neuman, W.F., and Mulryan, B.J. (1967) Synthetic hydroxyapatite crystals. III. The carbonate system. Calcified Tissue Research, 1, 94-104.

Neuman, W.F., Terepka, A.R., and Triffitt, J.T. (1968) Cycling concept of exchange in bone. Calcified Tissue Research, 2, 262-270.

610 Palmer, L.C., Newcomb, C.J., Kaltz, S.R., Spoerke, E.D., Stupp, S.I. (2008) Biomimetic systems
611 for hydroxyapatite mineralization inspired by bone and enamel. Chemical Reviews, 108,
612 4754-4783.
613 Paschalis, E.P., DiCarlo, E., Betts, F., Sherman, P., Mendelsohn, R., and Boskey, A.L. (1996)
614 FTIR microspectroscopic analysis of human osteonal bone. Calcified Tissue International,
615 59, 480-487.
616 Poyart, C.F., Bursaux, E., and Fréminet, A. (1975a) The bone CO_2 compartment: evidence for a
617 bicarbonate pool. Respiration Physiology, 25, 89-99.
618 Poyart, C.F., Fréminet, A., and Bursaux, E. (1975b) The exchange of bone CO_2 *in vivo*.
619 Respiration Physiology, 25, 101-107.
620 Rey, C., Collins, B., Goehl, T., Dickson, I.R., and Glimcher, M.J. (1989) The carbonate
621 environment in bone mineral: A resolution-enhanced Fourier transform infrared study.
622 Calcified Tissue International, 45, 157-164.
623 Rey, C., Renugopalakrishnan, V., Shimizu, M., Collins, B., and Glimcher, M.J. (1991) A
624 resolution-enhanced Fourier transform infrared spectroscopic study of the environment of
625 the CO_3^{2-} ion in the mineral phase of enamel during its formation and maturation. Calcified
626 Tissue International, 49, 259-268.
627 Rey, C., Combes, C., Drouet, C., and Glimcher, M.J. (2009) Bone mineral: update on chemical
628 composition and structure. Osteoporosis International, 20, 1013-1021.
629 Shimoda, S., Aoba, T., Moreno, E.C., and Miake, Y. (1990) Effect of solution composition on
630 morphological and structural features of carbonated calcium apatites. Journal of Dental
631 Research, 69, 1731-1740.
632 Suetsugu, Y., Shimoya, I., and Tanaka, J. (1998) Configuration of carbonate ions in apatite

633 structure determined by polarized infrared spectroscopy. Journal of the American Ceramic
634 Society, 81, 746-748.
635 Tacker, R.C. (2008) Carbonate in igneous and metamorphic fluorapatite: Two type A and two
636 type B substitutions. American Mineralogist, 93, 168-176.
637 Tyliszcak, T. (1992) BGAUSS Data Analysis Program. McMaster University.
638 Verbeeck, R.M.H., De Maeyer, E.A.P., and Driessens, F.C.M. (1995) Stoichiometry of
639 potassium- and carbonate-containing apatites synthesized by solid state reactions. Inorganic
640 Chemistry, 34, 2084-2088.
641 Verdelis, K., Lukashova, L., Wright, J.T., Mendelsohn, R., Peterson, M.G.E., Doty, S., Boskey,
642 A.L. (2007) Maturational changes in dentin mineral properties. Bone, 40, 1399-1407.
643 Vignoles, C. (1973) Contribution à l'étude de l'influence des ions alcalins sur la carbonatation
644 dans les sites de type B des apatites phosphor-calciques, thèse, L'université de Paul
645 Sabatier, Toulouse, France.
646 Wilson, R.M., Elliott, J.C., Dowker, S.E.P., and Smith, R. I. (2004) Rietveld structure refinement
647 of precipitated carbonate apatite using neutron diffraction data. Biomaterials, 25, 2205-
648 2213.
649 Yi, H., Balan, E., Gervais, C., Ségalen, L., Blanchard, M., and Lazzeri, M. (2014) Theoretical
650 study of the local charge compensation and spectroscopic properties of B-type carbonate
651 defects in apatite. Physics and Chemistry of Minerals, 41, 347-359.
652

(Figure Captions)

FIGURE 1. Orientation of type A carbonate ion in *c*-axis channel of sodium-bearing AB CHAP LM005: channel is defined by triclusters of Ca2 cations at unit-cell heights $z \approx 1/4$ (shaded) and $z \approx 3/4$ (open); note that displacement of O5 oxygen toward channel wall results in an additional short Ca2-O interaction (dashed lines); interatomic distances are Ångstroms and estimated standard deviations are in the third decimal place.

FIGURE 2. Broadscan infrared spectra of sodium-bearing AB CHAP LM005 and annealed carious enamel showing weak carbonate ν_3 absorption beyond 1500 cm^{-1} (after Arends and Davidson 1975; Fleet 2014b).

FIGURE 3. Asymmetric stretch (ν_3) region of infrared spectra for: (a) sodium-free AB CHAP PC55, with doublet bands labelled for carbonate ions in the apatite channel (type A and type A2) and calcium phosphate matrix (type B); (b) sodium-bearing AB CHAP LM005; and (c) sodium-free A CHAP PC71 (after Fleet and Liu 2007a).

FIGURE 4. Asymmetric stretch (ν_3) region of the FTIR spectrum for sodium-bearing AB CHAP LM005 fitted with overlapped Gaussian distributions corresponding to the peaks and shoulders evident in envelope: see also Table 4.

669

670

TABLE 1: Crystal synthesis experiments and amounts of sodium, A and B carbonate (pfu[a])

	EMPA	X-ray structure			IR(ν_2)
Experiment[b]	Na	A	B	B/A	B/A
Sodium-free A and AB CHAP					
PC71	-	0.75	0.11(2)	0.15	0.27
PC18	-	1.08(6)	0.49(2)	0.45	0.41
PC55	-	1.09(4)	0.56(2)	0.51	0.52
Sodium-bearing AB CHAP					
LM005	0.87(3)	1.00(5)	0.77(3)	0.77	0.78[c]
LM006	0.35(4)	0.52(3)	0.38(2)	0.73	0.81[c]

[a] pfu is per formula unit of $Ca_{10}(PO_4)_6X_2$. See Fleet (2012, 2014b) for more experimental details. [b] Range of *P* and *T* covered: 0.5-4.0 GPa, 1000-1500°C. [c] New IR measurement.

671

672

673

TABLE 2: Positions of infrared-active bands for carbonate in some apatites (cm^{-1})

Apatite	ν_3		ν_2	Type	Reference
Francolite	1453	1429	865	B	Elliott (1994, 1964)
Dahllite	1455	1416	873	B	Carlström (1968)
A CHAP	1537	1451	874	A	Bonel (1972)
A CHAP	1528	1463	878	A	Elliott (1994)
A CHAP, PC71	1544	1461	878	A	Fleet and Liu (2003)
B CHAP	1460	1420	871	B	Vignoles (1973)
B CHAP	1475	1419	873	B	Wilson et al. (2004)
AB CHAP, PC55	1569	1507	862	A2	Fleet and Liu (2004), Fleet (2009)
	1540	1449	879	A	
	1474	1409	870	B	
CFAP	1455	1429	866	B2	Shimoda et al. (1990)
Na AB CHAP	1500	1454	879	A	Nelson and Featherstone (1982)
	1469	1415	873	B	
Dental enamel	1545	1450	880	A	Elliott (1994, 1964)
	1465	1412	873	B	
Pig dental enamel	-	-	878	A	Rey et al. (1991)
	-	-	871	B	
	-	-	866	-	
Bone	1450	1409	877-865[a]		Baxter et al. (1966)
Fossil bone	1459	1429	872-866[a]		Baxter et al. (1966)

[a] Broad bands not well resolved.

674

675

676

677

678

679

TABLE 3: Change in relative proportions of carbonate species with aging Na-bearing AB CHAP containing HCO_3^- at low temperature[a]

	A	B	L	HCO_3^-	A+L GAIN	HCO_3^- LOSS
LM003						
quenched	26	39	9	27		
aged[b]	41	39	20	0	+26	-27
LM013						
quenched	40	32	10	17		
aged[c]	57	33	10	0	+17	-17
LM092						
quenched	22	48	1	29		
aged[d]	45	45	8	2	+30	-27

[a] Using out-of-plane bend (ν_2) band areas (after Fleet 2012). [b] 283 days at room temperature (RT), 55 days at 110°C. [c] 65 days at RT, 4 hours at 110°C. [d] 165 days at RT.

680

681

682

TABLE 4: Fitted bands for Na AB CHAP and estimated proportions of matrix (B) and channel (A) carbonate ions [1]

Carbonate	Absorption Band						Totals	B/A Ratio	
Type	1	2	6	4	3	5		IR(ν_3)	XRD
				LM005					
A	(1.6)	4.4	4.2	8.4			17.0	0.75[2]	0.77
B					6.4	6.4	12.8		
wavenumber	1536	1501	1389	1449	1474	1415		0.69[3]	
width	38	34	34	29	27	30		0.76[4]	
				LM006					
A	(1.2)	3.1	2.0	5.4			10.5	0.79[2]	0.73
B					4.1	4.2	8.3		
wavenumber	1530	1498	1390	1450	1472	1415		0.71[3]	
width	46	38	43	31	31	31		0.77[4]	
				LM002					
A	(0.2)	1.7	0.2	2.1			4.0	0.90[2]	-
B					1.8	1.8	3.6		
wavenumber	1534	1495	1387	1450	1468	1414		0.86[3]	
width	24	40	25	25	24	25		0.86[4]	

[1] Scale for band areas is arbitrary, and units for areas, wavenumbers and band widths (FWHH) are cm^{-1}; brackets flag overestimated values. [2] B/A calculated excluding area of band No. 1 for type A. [3] B/A calculated including area of band No. 1 for type A. [4] B/A calculated using average of bands 3 and 5 for type B and band No. 4 for type A.

683

684

685

686

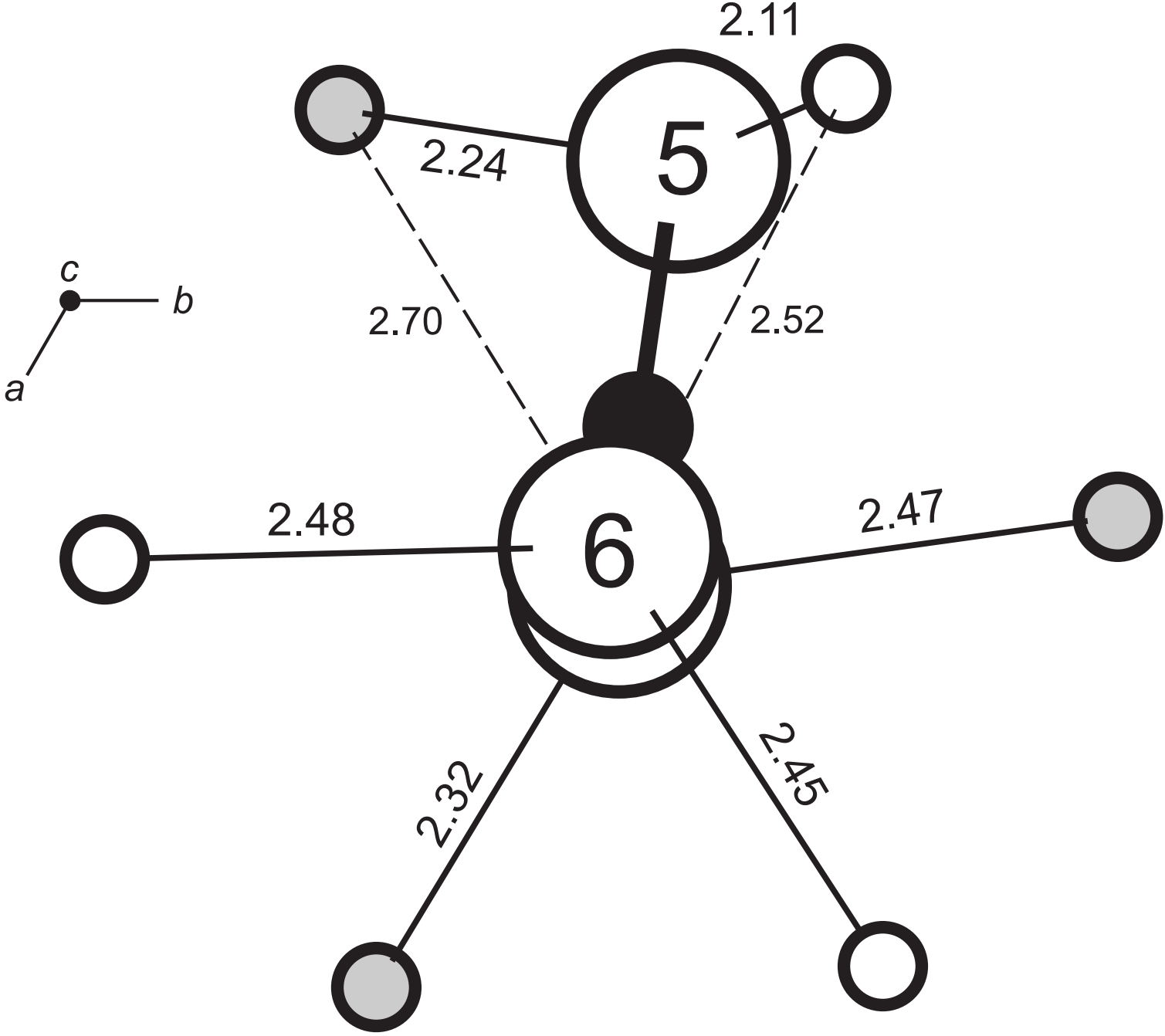
2.11
5
2.24
c
b
a
2.70
2.52
2.48
6
2.47
2.32
2.45

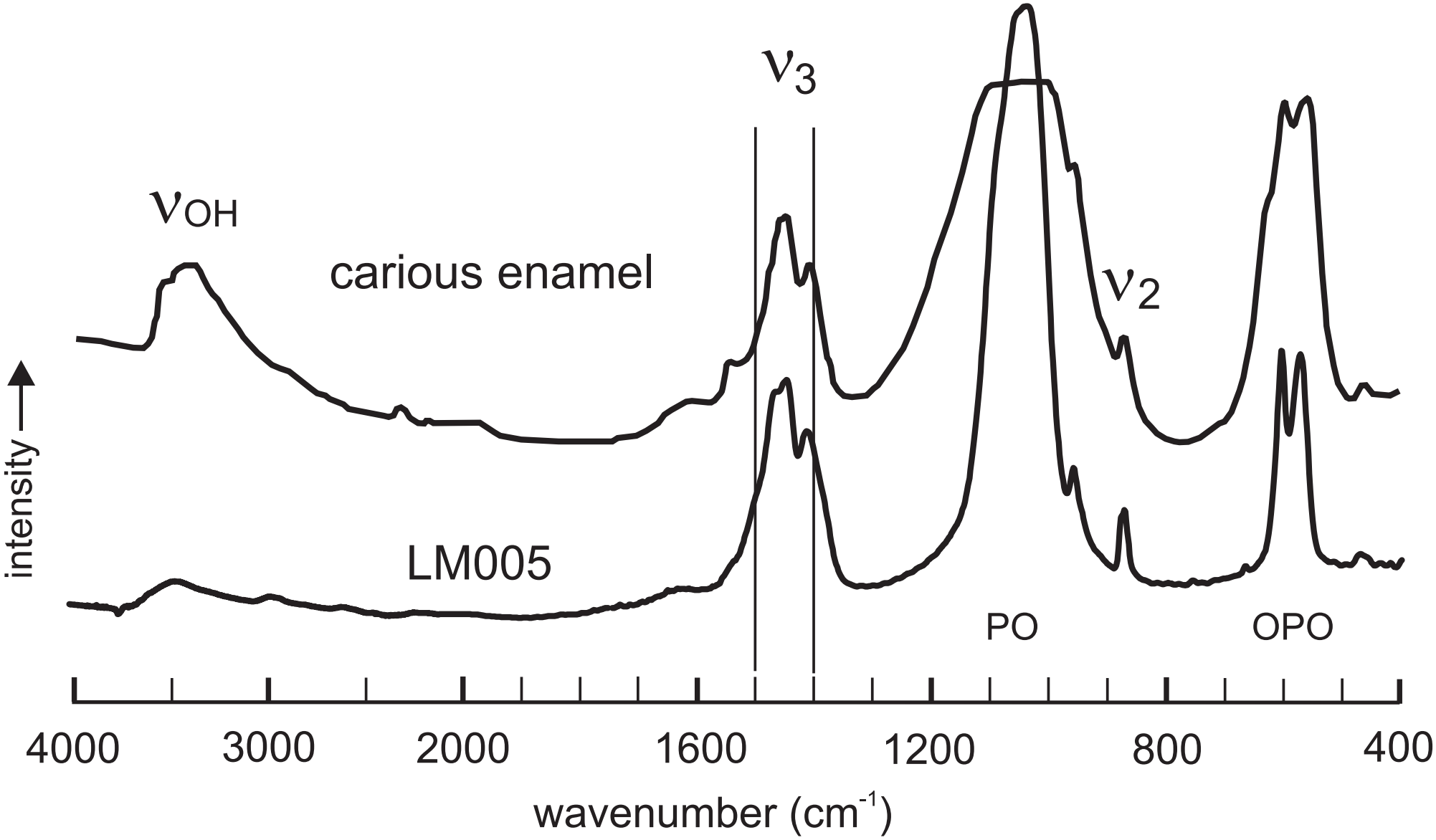
ν_3
ν_{OH}
carious enamel
ν_2
intensity
LM005
PO
OPO
4000
3000
2000
1600
1200
800
400
wavenumber (cm^{-1})

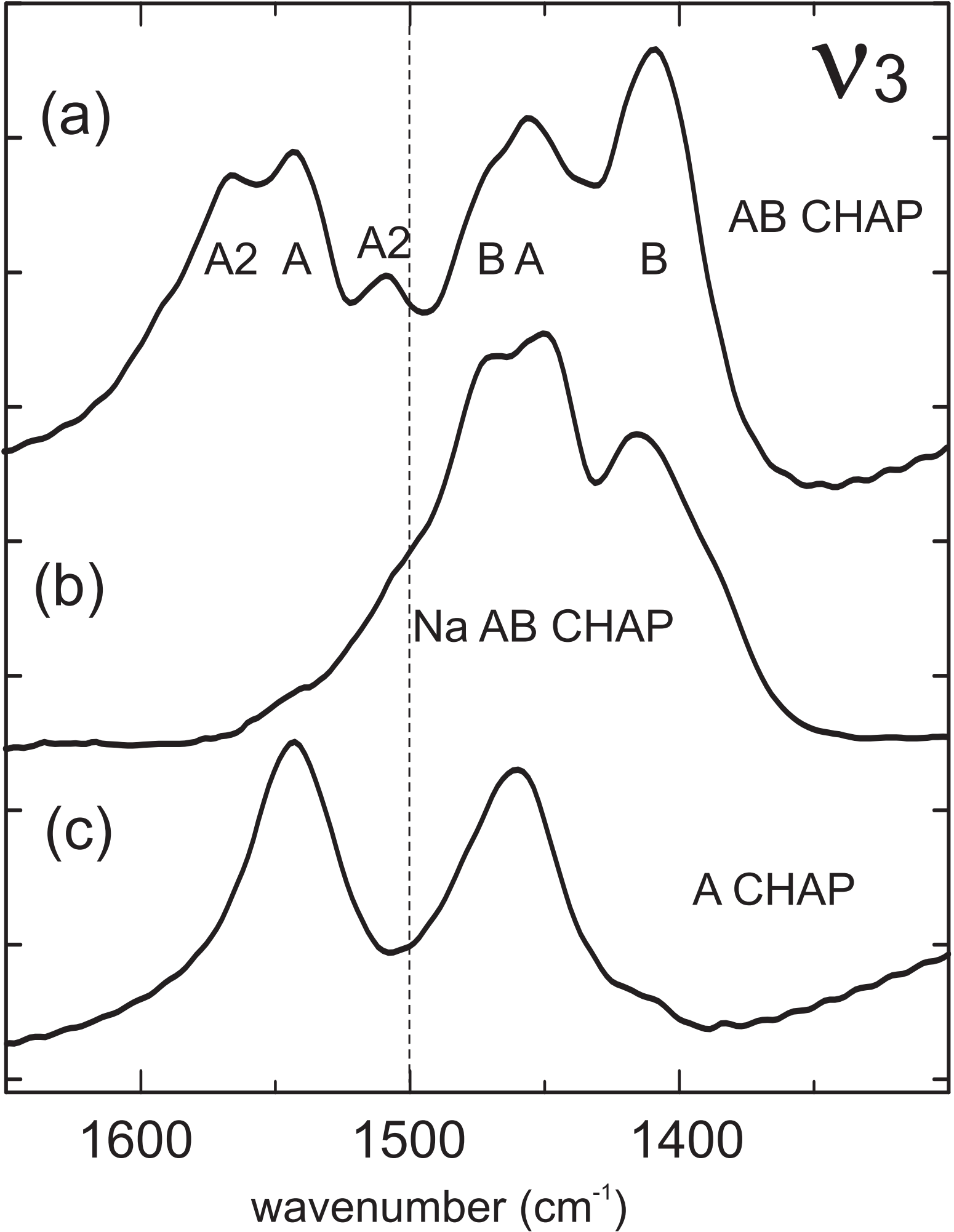
ν3
(a)
AB CHAP
A2
A
A2
B
A
B
(b)
Na AB CHAP
(c)
A CHAP
1600
1500
1400
wavenumber (cm-1)

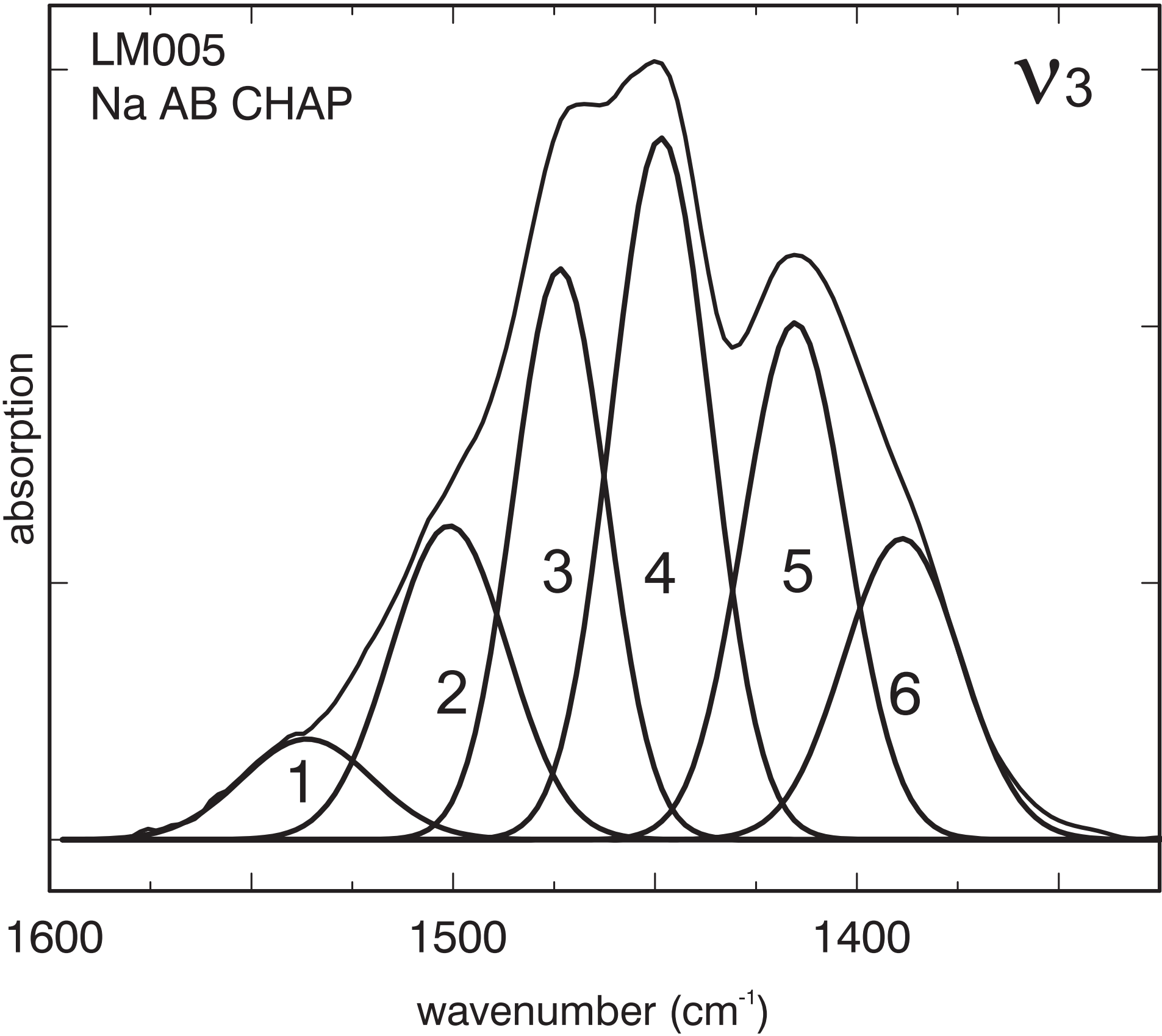
LM005
Na AB CHAP
ν3
absorption
1
2
3
4
5
6
1600
1500
1400
wavenumber (cm-1)